Journal of Colloid and Interface Science 543 (2019) 96–105

Contents lists available at ScienceDirect

Journal of Colloid and Interface Science

journal homepage: www.elsevier.com/locate/jcis

Regular Article

Efficient biofunctionalization of MoS_2 nanosheets with peptides as intracellular fluorescent biosensor for sensitive detection of caspase-3 activity

Xiao Li [a], Yuqing Li [a], Qiu Qiu [a], Qirui Wen [a], Qi Zhang [a], Wenjing Yang [a], Lihui Yuwen [a,*], Lixing Weng [b], Lianhui Wang [a,*]

[a] Key Laboratory for Organic Electronics and Information Displays and Jiangsu Key Laboratory for Biosensors, Institute of Advanced Materials (IAM), Jiangsu National Synergetic Innovation Centre for Advanced Materials (SICAM), Nanjing University of Posts and Telecommunications, 9 Wenyuan Road, Nanjing 210023, China
[b] School of Geography and Biological Information, Nanjing University of Posts and Telecommunications, Nanjing 210023, China

GRAPHICAL ABSTRACT

We develop a covalent biofunctionalization strategy of MoS_2 NSs with high conjugation efficiency of peptides for intracellular caspase-3 activity detection.

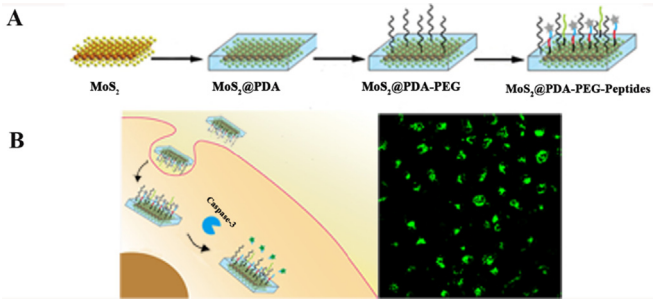

ARTICLE INFO

Article history:
Received 26 November 2018
Revised 18 January 2019
Accepted 4 February 2019
Available online 4 February 2019

Keywords:
MoS_2 NSs
Polydopamine
Caspase-3
Covalent biofunctionalization
Biosensor

ABSTRACT

Intracellular detection of caspase-3 activity is crucial for the study of cell apoptosis and caspase-3 related diseases. Although various nanomaterials-based biosensors have been constructed for this purpose, they often suffer from poor stability or complicated construction due to the lack of a facile and efficient biofunctionalization method, which decreases their sensing performance and limits their use in the complex physiological environments. As novel two-dimentional (2D) nanomaterials, MoS_2 nanosheets (NSs) have shown great potential for biosensing due to their unique properties. Herein, we develop a versatile yet facile covalent biofucntionalization strategy of MoS_2 NSs by utilizing polydopamine (PDA) as nano-bio interface, and construct an intracellular fluorescent biosensor (MoS_2@PDA-PEG-Peptide, MPPP) for the determination of caspase-3 activity. This covalent biofunctionalization of MoS_2 NSs can significantly improve the conjugation efficiency of biomolecules and enhance their stability in complicated environments, which is much better than conventional biofunctionalization by using thiol-metal coordination. Furthermore, this novel caspase-3 biosensor based on peptides biofunctionalized MoS_2 NSs shows high sensitivity and selectivity for the detection of caspase-3 with a limit of detection (LOD) of 0.33 ng/mL, and can be used for high-contrast fluorescent imaging of cell apoptosis.

* Corresponding authors.
E-mail addresses: iamlhyuwen@njupt.edu.cn (L. Yuwen), iamlhwang@njupt.edu.cn (L. Wang).

https://doi.org/10.1016/j.jcis.2019.02.011
0021-9797/

1. Introduction

Caspase-3, a cysteine-aspartic proteases, is a key mediator of apoptosis in various cells and its activation has been considered as an important hallmark that cells enter into the apoptosis process [1]. The deregulation of caspase-3 relates to various human diseases, such as cancers and neurodegenerative diseases, and the in situ detection of caspase-3 activity in cells is essential to study the cell apoptosis process of these diseases [2,3]. As a powerful technique for the intracellular detection of biomolecules and visualization of biological processes, fluorescent biosensing has been used for the determination of intracellular caspase-3 activity owing to their high sensitivity, specificity, and versatility [4–7].

Recently, nanomaterials with excellent fluorescence emitting or quenching properties have been explored as fluorescent biosensors for the detection of caspase-3 activity [3,8–10]. In order to construct nanobiosensors, several biofunctionalization methods have been used to conjugate biomolecules to functionalize nanomaterials, such as metal-affinity coordination and carbodiimide crosslinking chemistry (EDC/NHS). For example, thiol terminated peptides have been conjugated to the surface of metal nanomaterials, including Au nanoparticles, [11] Au nanoclusters, [12] Au nanorods, [13] and etc., to construct intracellular protease biosensors via thiol-metal coordination. However, thiol-metal coordination is not strong enough and thiol-terminated peptides can be displaced by intracellular thiol-containing biomolecules through thiol exchange reaction, resulting in non-specific signals [14]. Besides, Medintz et al. utilized EDC/NHS chemistry to activate carboxylic acid groups on quantum dots (QDs) for covalently conjugating peptides [15]. Wang et al. used the similar method to construct peptides functionalized graphene oxide (GO) biosensor for the detection of caspase-3 activity [8]. However, EDC/NHS activation method often suffers from complicated operation and low efficiency. Hence, a facile and efficient biofunctionalization method to construct peptides conjugated nanobiosensors for intracellular caspase-3 activity detection is still needed.

MoS_2 nanosheets (NSs), as an inorganic graphene analog, is made up of a layer of Mo atoms sandwiched between two layers of S atoms [16]. Owing to their high surface-to-volume ratio, strong fluorescence quenching ability, and excellent biocompatibility, MoS_2 NSs have been widely used to construct various biosensors for the detection of enzymes, proteins, nucleic acids, glucose, and so on [17–19]. Nonetheless, proper surface functionalization is still essential to enable them with required biological functions and colloidal stability. Up to now, many biofunctionalization methods have been developed for the construction of MoS_2 NSs-based biosensors, including hydrophobic interaction, van der Waals force, electrostatic attraction, and thiol coordination [20–22]. Nevertheless, these interactions are non-covalent and relatively weak, and the detachment of biomolecules from MoS_2 NSs is inevitable, which may seriously influence the sensitivity, stability, specificity, and biocompatibility of the MoS_2 NSs-based biosensors, and greatly limit their application in complicated environments, especially for the intracellular sensing [21–24]. Therefore, it is necessary to develop an efficient biofunctionalization approach to construct high-performance biosensors based on MoS_2 NSs.

Polydopamine (PDA), a mussel-inspired polymer, has been recognized as the most versatile materials for surface functionalization of almost all kinds of materials [25]. Besides their excellent adhesive ability and facile coating process, PDA also has plenty of reactive catechol groups which greatly facilitate further chemical reactions with thiol-terminated biomolecules via facile Michael addition reaction [25–27]. Therefore, PDA coating provides a feasible way for covalent biofunctionalization of nanomaterials, holding great potential in constructing high-performance biosensors.

Herein, we developed a covalent biofucntionalization strategy of MoS_2 NSs for efficient conjugation of peptides by utilizing PDA as nano-bio interface, and constructed an intracellular fluorescent biosensor for the determination of caspase-3 activity. As shown in Scheme 1a, after PDA coating and PEGylation, fluorescein (FAM)-labelled substrate peptide with caspase-3 specific cleavage sequence DEVD (Asp-Glu-Val-Asp) and cell-penetrating peptide (TAT), are conjugated to MoS_2@PDA NSs covalently via Michael addition reaction between thiol groups from peptides and catechol groups of PDA. This MoS_2@PDA-PEG-Peptide (MPPP) biosensor is based on fluorescence resonance energy transfer (FRET) with FAM as donor and MoS_2 NSs as acceptor. During cell apoptosis, caspase-3 is activated to cleave the substrate peptide and the FAM is released from MoS_2 NSs (Scheme 1b), which results in the fluorescence recovery of the MPPP biosensor and enables the visualization of the intracellular apoptosis process.

2. Experimental section

2.1. Materials and characterizations

Molybdenum (IV) sulfide (MoS_2) powder (<2 μm, 99%), recombinant human caspase-3 (active form, 10 μg), bovine serum albumin (BSA), human serum albumin (HSA), L-Glutathione reduced and transferrin human were purchased from Sigma-Aldrich (USA). The n-butyllithium (n-BuLi, 2.4 M heaxane solution) was obtained from Amethyst (China). Methoxy-poly(ethylene glycol) with a thiol group (PEG-SH, MW = 5000) was obtained from JenKem Technology Co. Ltd. (China). Caspase-3 inhibitor (Z-DEVD-FMK) and Caspase-3 Colorimetric Assay Kit were purchased from R&D Systems (USA). Staurosporine (STS) and 3-[(3-cholamidopropyl) dimethylammonio]-1-propanesulfonic acid (CHAPS) were purchased from MedChem Express (USA). Lactate dehydrogenase (LDH)-Cytotoxicity Assay Kit was purchased from Biovision (USA). Synthetic peptides including FAM-labelled caspase-3 substrate peptide (CCKKGGDEVDK-FAM, P1) and cell-penetrating peptide (CCKKGGGRKKRRQRRR, P2) were obtained from GL Biochem (China). Dopamine hydrochloride was purchased from Alfa Aesar (USA). All of other reagents were of analytical grade. All solutions were prepared using ultrapure water (18.2 MΩ, Millipore).

Transmission electron microscopy (TEM) images were obtained by HT7700 (Hitachi, Japan) with acceleration voltage of 120 kV. Atomic force microscopy (AFM) images were acquired on Nanoscope IIIa (Bruker, USA). The UV–vis-NIR absorption spectra were recorded on a UV-3600 spectrophotometer (Shimadzu, Japan). Photoluminescence spectra were obtained using a RF-5301PC spectrophotometer (Shimadzu, Japan). X-ray photoelectron spectroscopy (XPS) was performed on a PHI 5000 VersaProbe with an A1 Kα (hυ = 1486.6 eV) X-ray source (Ulvac-Phi, Japan) [28]. Measurements were taken at a taken-off angle of 45 °C with respect to the sample surface. Infrared spectra were obtained from a Perkin-Elmer 1600 series FT-IR spectrophotometer. The Zeta potential of the nanosheets were all recorded on a ZetaPALS Potential Analyzer (Brookhaven, America). CLSM images were taken on Olympus FLUOVIEW 1000 (Olympus, Japan). Flow cytometry analysis was conducted on FlowSight Imaging Flow Cytometer (Merck Millipore, Germany).

2.2. Preparation of MoS_2 NSs and PDA coated MoS_2 (MP) NSs

Monolayer MoS_2 NSs were exfoliated from the bulk MoS_2 powder by ultrasonication enhanced lithium intercalation approach reported in our previous work [29]. The PDA coated MoS_2 (MP) NSs were prepared by ultrasonication assisted polymerization of

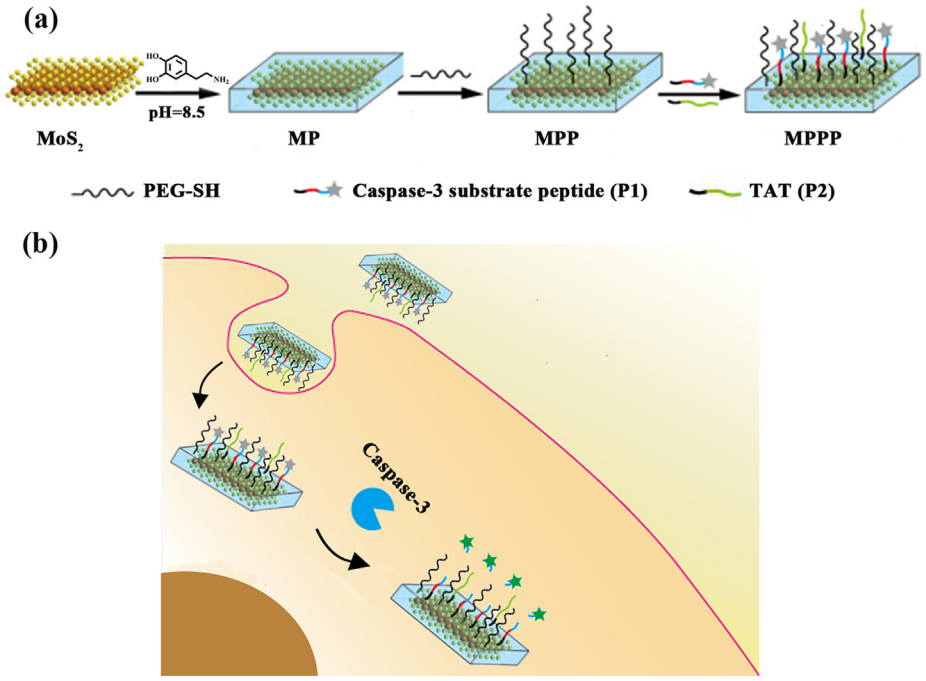

Scheme 1. (a) Preparation of polydopamine coated MoS_2 (MoS_2@PDA NSs, MP NSs), subsequently PEG modification (MoS_2@PDA-PEG NSs, MPP NSs), and finally the construction of peptides biofunctionalized biosensor (MoS_2@PDA-PEG-Peptide NSs, MPPP NSs). (b) Schematic illustration for intracellular caspase-3 detection based on MPPP biosensor in apoptotic cells.

dopamine at a weak alkaline condition. Typically, 10 mL of MoS_2 NSs aqueous dispersion (100 μg/mL) was added into 40 mL of Tris-HCl buffer (10 mM, pH = 8.5) with stirring. Then 5.9 mg of dopamine hydrochloride was added and subsequently the mixed solution underwent ultrasonication (53 kHz, 180 W) for 1 h. The MP NSs were collected after centrifugation at 12,000 rpm for 30 min and washed with ultrapure water for three times.

2.3. Preparation of MPP NSs and construction of the MPPP biosensor

The thiol-terminated PEG conjugated MP NSs (MPP NSs) were prepared by adding 30 mg PEG-SH into 21 mL of Tris-HCl solution (10 mM, pH = 8.5) containing 6 mL of 160 μg/mL of MP NSs. Then the reaction mixture was stirred at room temperature for 12 h. After that, the mixture was centrifuged at 12,000 rpm for 30 min. The obtained precipitates were dispersed in ultrapure water and centrifuged for another three times. For construction of the MPPP biosensor, 92.4 μL of 1 mg/mL P1 and 59.2 μL of 1 mg/mL P2 were added into 21 mL of 10 mM Tris-HCl solution (pH = 8.5) containing 3 mL of 160 μg/mL MPP NSs. After the mixture being stirred for 12 h at 37 °C, excessive peptides were removed by repeated centrifugations at 21,000 rpm for 15 min. The obtained precipitates were dispersed in Tris-HCl buffer (10 mM, pH = 8.5) and centrifuged until there was no fluorescence in the supernatant. The final product of MPPP NSs was dispersed in ultrapure water and stored at 4 °C.

2.4. Evaluating the efficiency of peptide conjugation to MoS_2 NSs or MoS_2@PDA NS

Firstly, MoS_2-P1 and MoS_2@PDA-P1 NSs were prepared by adding 120 μL of MoS_2 NSs or MoS_2@PDA NSs (100 μg/mL) into 849 μL of Tris-HCl solution (10 mM, pH = 8.5) containing 31 μL of P1 (1 mg/mL), and then the reaction mixtures were stirred at 600 rpm for 12 h at 37 °C. After that, the mixtures were centrifuged at 21,000 rpm for 20 min. The obtained precipitates were dispersed in Tris-HCl solution (10 mM, pH = 8.5) and centrifuged for several times. Then MoS_2-P1, MoS_2@PDA-P1, MoS_2 and MoS_2@PDA NSs with the same concentration of MoS_2 were characterized by UV–vis-NIR spectroscopy at 495 nm. The relative efficiency of peptides conjugated to MP NSs or MoS_2 NSs was calculated as follows:

$$\eta = \frac{A_{MoS2@PDA-P1} - A_{MoS2@PDA}}{A_{MoS2-P1} - A_{MoS2}} \times 100\%$$

2.5. Quantify the coverage of PEG-SH on the surface of MP NSs

Briefly, 24 μL of MP NSs (1 mM) were reacted with different concentrations of PEG-SH (final concentrations ranging from 0.06 mM to 30 mM). After being centrifuged at 21,000 rpm for 20 min and washed for another three times, the collected supernatants were diluted to 800 μL. Then 50 μL aliquot of the supernatant was added to phosphate buffer (0.1 M, pH = 8.0, 1415 μL), and 35 μL of Ellman's reagent (5 mg/mL in the phosphate buffer) was subsequently added and mixed for 10 min. The absorbance of the mixture at 412 nm was measured and the concentration of thiol group (PEG-SH) was acluculated according to a standard curve. The coverage rate of PEG-SH on MP NSs can be calculated as follows: $\xi = n/n_m$, where n represents the amount of PEG-SH conjugated to MP NSs, and n_m represents the maximum amount of PEG-SH that can fully occupy the available catechol sites on MP NSs.

2.6. In vitro detection of caspase-3 activity using MPPP biosensor

In a typical caspase-3 activity assay, 12.5 μL of MPPP biosensor (160 μg/mL) was diluted to 8 μg/mL by caspase-3 assay buffer (containing 50 mM HEPES (pH = 7.4), 100 mM NaCl, 1 mM EDTA, 10% glycerol, and 0.1% CHAPS), then different volumes of caspase-3 (final concentrations ranging from 0, 2, 4, 8, 16, 32, 48, 60, 120, 240, to 360 ng/mL) were added and incubated at 37 °C for 12 h. As controls, the MPPP biosensor was incubated without

caspase-3, or it was pretreated with Z-DEVD-FMK (100 μM) and then incubated with caspase-3 (360 ng/mL) for 60 min at 37 °C. Then the time-dependent fluorescence spectra of the MPPP biosensor were recorded after the addition of 45 μL of caspase-3 (2 μg/mL) to 192.5 μL of caspase-3 assay buffer containing 12.5 μL of the MPPP biosensor (160 μg/mL) at scheduled time points. The selectivity was evaluated by incubating MPPP biosensor with caspase-3 (10 nM) and other species including BSA, HSA, GSH, pepsin, L-cysteine, and transferrin of 1 μM at 37 °C for 60 min. The fluorescence spectra were collected from 500 to 620 nm with the excitation wavelength of 480 nm.

2.7. Cell culture

The human cervical carcinoma (HeLa) cells were obtained from KeyGEN BioTECH. HeLa cells were cultured in DMEM medium (KeyGEN BioTECH) in a humidified incubator at 37 °C with 5% CO_2. The medium was supplemented with 10% fetal bovin serum (FBS, Cellsera), 0.08 mg/mL streptomycin and 80 U/mL penicillin.

2.8. Cytotoxicity assessment of the MPPP biosensor

The cytotoxicity of the MPPP biosensor was evaluated by the LDH-Cytotoxicity Assay Kit. Briefly, HeLa cells were seeded on the 96-well plate with the density of 1.0×10^4 per well and incubated for 12 h, and then the culture medium was replaced with 100 μL MPPP biosensor of different concentrations (0, 4, 8, 16, 32, 64, 128 μg/mL) suspended in the fresh DMEM medium without FBS. Notably, HeLa cells cultured without any MPPP biosensor were set as the low control, and cells cultured with DMEM medium containing 1% Triton X-100 acted as the high control. After incubating for 24 h, 50 μL of supernatant in each well was transferred cautiously into an optical clear 96-well plate, and 100 μL of reaction mixtures (containing 0.25 mL of catalyst solution and 11.25 mL of dye solution) were added to each well. The plate was incubated for 30 min at room temperature in the dark. The absorbance of all samples was measured at 495 nm using a microtiter plate reader (PowerWave XS2). The viability of cells was calculated using the formula as follows:

$$\textit{Cell viability}\ (\%) = 100\% - \frac{\textit{test sample} - \textit{low control}}{\textit{high control} - \textit{low control}} \times 100\%$$

2.9. Colorimetric assay of caspase-3 activity in cell extracts

HeLa cells (5.0×10^5) were plated in 35 mm-diameter cell culture dishes and incubated with 2 μM of staurosporine (STS) for 2 h to induce apoptosis. Cells were washed gently with cold PBS (10 mM, pH = 7.4) and collected by centrifugation in conical tubes at 500 rpm for 2 min. After gently removed the supernatants, the cell pellets were lysed by the addition of lysis buffer (25 μL per 10^6 cells) and incubated on ice for 15 min. Following centrifugation at 10,000 rpm for 10 min, the supernatants were transferred to new tubes and kept on ice. The enzyme reaction for caspase-3 activity was performed in a 96 well flat bottom microplate with each well containing 60 μL of cell lysate, 50 μL of reaction buffer, and 2.5 μL of caspase-3 colorimetric substrate (DEVD-pNA). Finally, the mixtures were incubated at 37 °C for 2 h, and afterwards detected by a microtiter reader at the wavelength of 405 nm. All of the experiments were repeated at least for three times.

2.10. Confocal laser scanning microscope (CLSM) imaging of cell apoptosis

HeLa cells (2.0×10^4) were seeded into confocal dishes with 10 mm bottom well for 24 h. When the cells were about 80% confluent, they were washed with PBS (10 mM, pH = 7.4) for three times and treated with fresh culture medium containing 8 μg/mL of MPPP biosensor. After incubation for 3 h, the medium was removed and each dish was washed twice with cold PBS (10 mM, pH = 7.4). After that, the medium was replaced with fresh medium containing STS (2 μM) and incubated for 4 h at 37 °C. For inhibitor group, Z-DEVD-FMK (100 μM) was used to pretreat HeLa cells for 1 h before the addition of STS (2 μM, 4 h). For the negative group, neither STS nor Z-DEVD-FMK was involved. Subsequently, the cells were visualized on a confocal laser scanning microscope. The fluorescence of released FAM in HeLa cells was collected from 500 nm to 600 nm with 488 nm excitation.

2.11. Flow cytometry for caspase-3 activity detection

HeLa cells (5.0×10^5) were plated in 35 mm-diameter cell culture dishes for 24 h and then incubated with the MPPP biosensor (8 μg/mL) for 3 h. Meanwhile, HeLa cells without any treatment served as control. After being washed twice by the cold PBS (10 mM, pH = 7.4), cells were incubated with STS (2 μM) for another 4 h at 37 °C. As for the inhibitor group, cells were pretreated with Z-DEVD-FMK (100 μM) for 1 h and then incubated with STS (2 μM) for 4 h. Then the HeLa cells were digested, collected, and resuspended in fresh DMEM medium, and the collected cells were analyzed by flow cytometry.

3. Results and discussion

3.1. Biofunctionalization of MoS_2 NSs and the construction of Caspase-3 biosensor

Monolayer MoS_2 NSs were exfoliated from natural MoS_2 powder by ultrasonication enhanced lithium intercalation method [29]. Then PDA was coated on the surface of MoS_2 NSs via ultrasonication assisted polymerization of dopamine to prepare MoS_2@PDA nanosheets (MP NSs). To further enhance the biocompatibility and reduce the nonspecific adsorption, thiol-terminated poly (ethylene glycol) (PEG-SH) was conjugated to the surface of MoS_2@PDA NSs to form MoS_2@PDA-PEG nanosheets (MPP NSs). Then, dye-labelled substrate peptide (CCKKGGDEVDK-FAM, P1) with caspase-3 specific cleavage site and cell-penetrating peptide (TAT, CCKKGGGRKKRRQRRR, P2) were conjugated to MPP NSs to form MPPP NSs via Michael addition reaction between thiol groups from peptides and catechol groups of PDA. The cell-penetrating peptide (TAT) with positive charge can be utilized to improve the efficiency of intracellular delivery and endosomal escape [30,31].

The morphology of the as-prepared MoS_2 NSs, MP NSs, MPP NSs, and MPPP NSs were characterized by TEM and AFM. As the TEM images and size distribution stastics histograms shown in Fig. 1a–d and Fig. S1a–d, all of the samples have uniform sheet-like morphology with the average sizes ranging from about 188 nm to 208 nm. The AFM image (Fig. 1e and Fig. S1e) shows that the thickness of MoS_2 NSs before surface functionalization is about 1.32 nm, which is consistent with previously reported thickness of the monolayer MoS_2 NSs prepared by chemical exfoliation [29,32]. The thickness of MP NSs (Fig. 1f and Fig. S1f) and MPP NSs (Fig. 1g and Fig. S1g) increases to about 5.18 nm and 5.70 nm, due to the coating of PDA and PEG, respectively. Moreover, the average thickness of the MPPP NSs (Fig. 1h and Fig. S1h) further increases to about 7.67 nm, which can be ascribed to the successful conjugation of caspase-3 substrate peptide (P1), TAT peptide (P2), and PEG [8].

The ultraviolet-visible-near infrared (UV–vis-NIR) spectra of MoS_2 NSs, MP NSs, MPP NSs and MPPP NSs are showed in Fig. 2a. There is a broad absorption band of the monolayer MoS_2 NSs from UV to NIR region [21]. After PDA coating, the absorbance

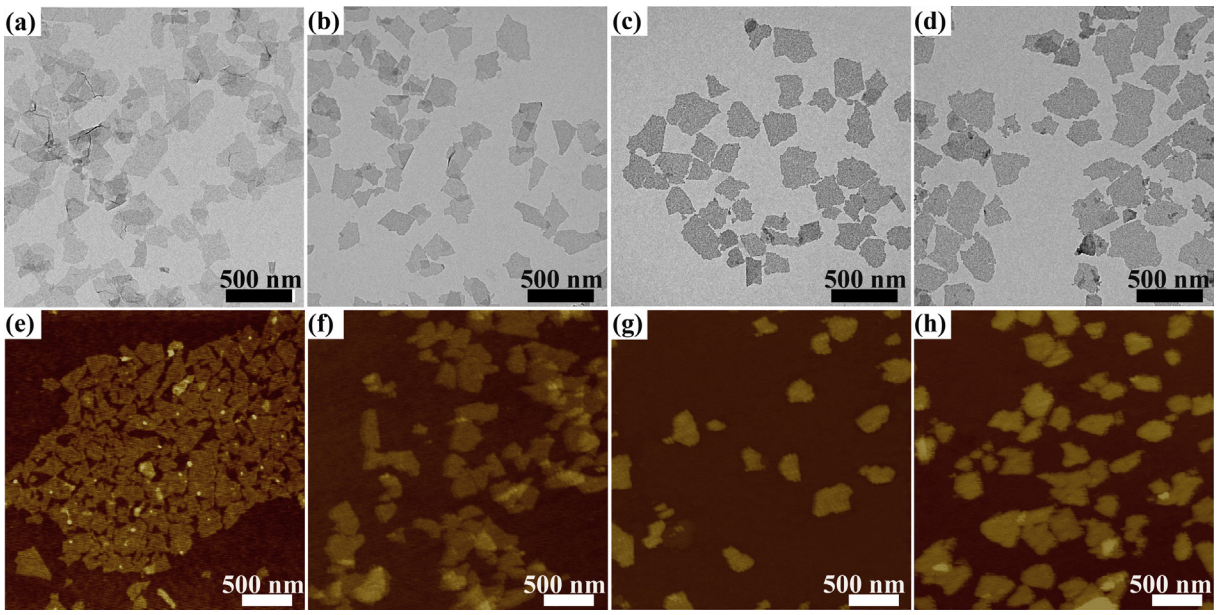

Fig. 1. Transmission electron microscopy (TEM) images (a–d), and atomic force microscopy (AFM) images (e–h) of MoS_2 NSs (a, e), MP NSs (b, f), MPP NSs (c, g) and MPPP NSs (d, h).

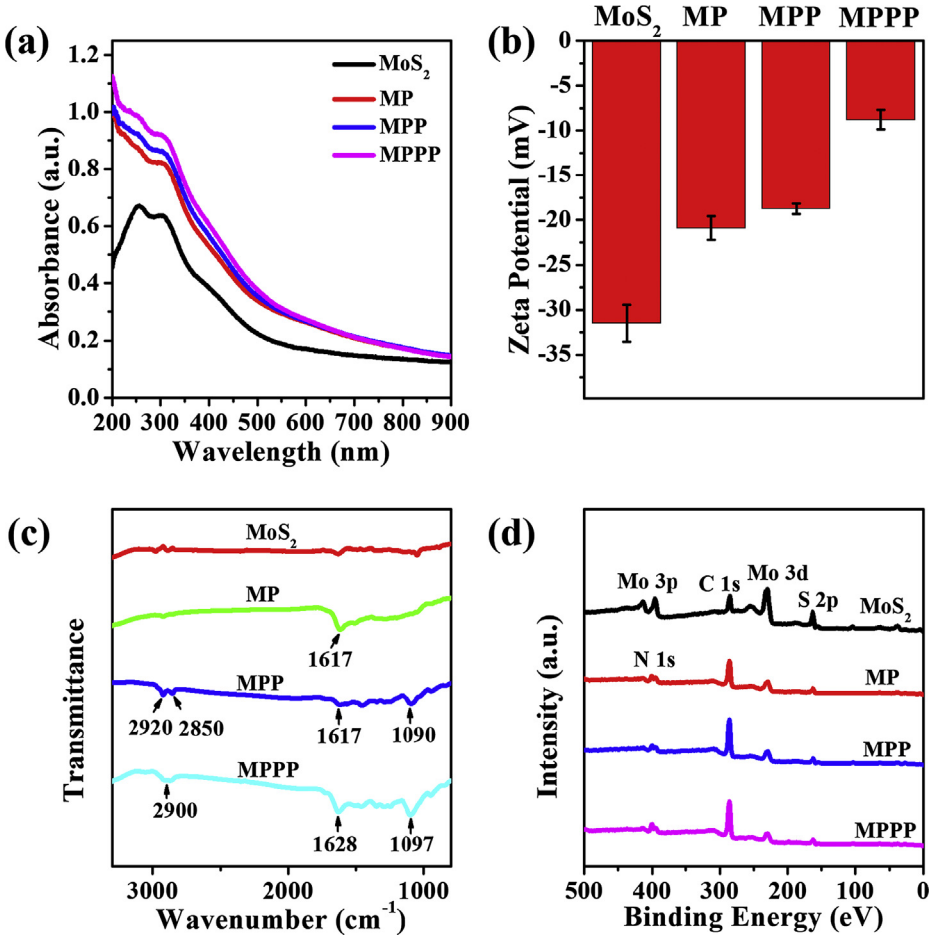

Fig. 2. (a) Ultraviolet–visible-near infrared (UV–vis-NIR) absorption spectra, (b) Zeta potential, (c) Fourier transform infrared spectroscopy (FT-IR) spectra, and (d) X-ray photoelectron spectroscopy (XPS) spectra of MoS_2 NSs, MP NSs, MPP NSs, and MPPP NSs. The values of zeta potential are presented as average ± standard deviation (S.D.) from three independent measurements.

of MP NSs slightly increases, resulting from the polymerized dopamine [25]. As shown in Fig. 2b, the zeta potential of MoS_2 NSs is about −31.5 mV, which shifts to −20.8 mV after PDA coating, due to the deprotonation of phenolic hydroxyl groups of PDA and the shielding effect [25,33–34]. With the modification of PEG, the zeta potential of MPP NSs further increases to −18.7 mV, which originates from the existence of electroneutral PEG. After the conjugation of peptides, the zeta potential of MPPP NSs further increases by 10 mV with respect to MPP NSs, which can be ascribed to the positive charge of TAT [31]. Then Fourier transform infrared (FT-IR) spectroscopy is used to verify the chemical structures of MoS_2 NSs, MP NSs, MPP NSs, and MPPP NSs. As shown in Fig. 2c, in contrast with the as-prepared MoS_2 NSs, the additional IR peak for MP NSs at 1617 cm^{-1} originates from the bending vibration of N—H and the stretching vibration of C=C, [34,35] suggesting the presence of PDA on the MoS_2 NSs. After PEG conjugating, the newly emerged IR peaks at 2850 cm^{-1}, 2920 cm^{-1}, and 1090 cm^{-1} can be assigned to the symmetric stretching of C—H, the asymmetric stretching of C—H, and the stretching vibrations of C—O—C, respectively, [36] confirming the successful conjugation of PEG to MP NSs. Furthermore, for MPPP NSs, the IR absorption bands at 2900 cm^{-1} and 1628 cm^{-1} result from the C—H stretching [8] and β-sheet of amide I [37], respectively, demonstrating the successful peptide biofunctionalization of MPP NSs. X-ray photoelectron spectroscopy (XPS) is used to further analyze the compositions and chemical states of the MoS_2 NSs after different surface functionalization methods. As shown in Fig. 2d, the survey XPS spectra indicates that MoS_2 NSs are composed of Mo and S elements with peaks located at about 413 eV, 395 eV, 229 eV, and 162 eV, which are corresponding to Mo $3p_{1/2}$, Mo $3p_{3/2}$, Mo 3d, and S 2p, respectively [21,38]. Owing to the coating of PDA on MoS_2 NSs, the peak intensities of Mo and S decrease in MP NSs. The appearance of the N 1s peak at 400 eV further confirms the existence of PDA on MoS_2 NSs [34,39]. According to the binding energies of carbon species and sulfur species shown in Table S1, the C 1s and S 2p core-level XPS spectrums can be deconvoluted into four components and five components, respectively [26,40–42]. As shown in Fig. S2 and Table S2, the content of C—O bond in MPP NSs (37.25%) significantly increased in comparison with MP NSs (13.14%), verifying the successful conjugation of PEG-SH on MP NSs. Moreover, the contents of C=O bond in MP NSs (25.07%), MPP NSs (16.03%), and MPPP NSs (12.38%) gradually decreased, which can be ascribed to the conversion of oxidized quinone groups to catechol groups during the Michael addition reaction between thiol groups both in PEG and peptides and PDA in MP NSs [25]. As shown in Fig. S3, after peptide biofunctionalization, higher content of C—S bond in MPPP NSs (11.85%) than that in MPP NSs (4.08%) further verifies the successful conjugation of peptides on MPP NSs.

3.2. Efficient covalent biofunctionalization of MoS_2 NSs with PDA as nano-bio interface

Due to the inert nature of atoms in the basal plane of MoS_2 NSs, biofunctionalization of MoS_2 NSs by non-covalent interaction is not reliable. Since PDA possesses both excellent adhesive capability and versatile reactivity, it can serve as a nano-bio interface to integrate biomolecules with MoS_2 NSs under mild reaction conditions. The efficiency of covalent biofunctionalization of MoS_2 NSs with PDA as interface was compared with the biofunctionalization by using thiol-metal coordination. P1 biofunctionalized MoS_2 NSs (MoS_2-P1) via thiol-metal coordination and P1 biofunctionalized MoS_2@PDA NSs (MoS_2@PDA-P1) by covalent bond were prepared with the same concentration of MoS_2. The UV–vis-NIR spectra of P1, MoS_2-P1 NSs, MoS_2@PDA-P1 NSs, MoS_2 NSs, and MoS_2@PDA NSs were measured. As shown in Fig. 3a, P1 has an obvious characteristic absorption peak at 495 nm originating from fluorescein (FAM). Compared with MoS_2 NSs and MoS_2@PDA NSs, the increased absorbance at 495 nm of MoS_2-P1 NSs and MoS_2@PDA-P1 NSs verifies the successful conjugation of P1. According to the Lambert-Beer law, the amounts of P1 conjugated to the MoS_2 NSs or MoS_2@PDA NSs can be calculated. As shown in Table S3, the amount of peptides conjugated to MoS_2@PDA NSs by covalent biofunctionalization method is 3.08 times to that of MoS_2 NSs via thiol-metal coordination, indicating high conjugation efficiency of covalent biofunctionalization of MoS_2 NSs by using PDA as nano-bio interface. Moreover, we also evaluated the coverage rate of PEG-SH on MP NSs by using Ellman's assay [43–44]. As shown in Fig. S4, the amount of PEG-SH conjugated to MP NSs gradually increases with the amount of the added PEG-SH and reaches the maximum near the molar ratio of 200:1 ($n_{PEG\text{-}SH}$:n_{MoS2}) due to the complete occupation of the available catechol sites by PEG-SH. Thus, PEG-SH coverage rate on MP NSs during the step of PEG modification is calculated to be about 1.4%, indicating adequate reactive catechol sites are still remained for further conjugation of peptides.

Furthermore, the colloidal stability of MoS_2 NSs using different biofunctional methods was evaluated. After PEG modification, peptides (P1 and P2) were further conjugated to MoS_2 NSs via thiol-metal coordination and MoS_2@PDA NSs by covalent bond, respectively. The colloidal stability of MoS_2-PEG-P1/P2 nanosheets (MPP' NSs) and MoS_2@PDA-PEG-P1/P2 nanosheets (MPPP NSs) were evaluated in fetal bovine serum (FBS), phosphate buffer saline (PBS, pH = 7.4), and Dulbecco's modified Eagle medium (DMEM). As shown in Fig. 3b, MPP' NSs almost aggregated completely at the concentration of 20 μg/mL (MoS_2) after 36 h storage at 4 °C. In contrast, MPPP NSs stayed clear, and no aggregation was observed even after one month storage. The greatly enhanced colloidal stability of MPPP NSs can be ascribed to the high conjugation efficiency of thiol-PEG by covalent biofunctionalization. Taken together, PDA provides an efficient and versatile nano-bio interface for biomolecules conjugation to MoS_2 NSs, and can improve the stability of MoS_2 NSs-based biosensors, suggesting the distinct advantage of covalent biofunctionalization strategy compared to non-covalent biofunctionalization method.

3.3. In vitro detection of caspase-3 activity

In order to study the validity of the MPPP biosensor for caspase-3 detection, *in vitro* enzymatic assays were performed. As shown in Fig. 4a, the MPPP biosensor retains "off" state owing to the efficient FRET from FAM to MP NSs, whereas the fluorescence intensity at 518 nm increases significantly after the addition of caspase-3, due to the specific cleavage of peptide sequence DEVD by caspase-3, resulting in the release of FAM from MPPP NSs and subsequent recovery of fluorescence. Additionally, in the presence of caspase-3 inhibitor (Z-DEVD-FMK), only very weak fluorescence is observed, suggesting that the fluorescence recovery is a caspase-3 specific event. Then the time-dependent fluorescence response of MPPP biosensor was investigated. Fig. 4b shows that the fluorescence intensity of MPPP biosensor gradually increases with the presence of caspase-3 and reaches its maximum at 60 min. The response time of the MPPP biosensor is 60 min, which is similar to other fluorescent caspase-3 nanobiosensors [9,13,45–47]. As shown in Fig. 4c, the fluorescence intensity enhances linearly with the increased concentration of caspase-3 and the linear range is from 2 ng/mL to 360 ng/mL with a limit of detection (LOD) of 0.33 ng/mL, which is better than previous reports of intracellular fluorescent caspase-3 biosensors (Table S4) [8–10,47]. Furthermore, the specificity of the MPPP biosensor was evaluated by measuring the fluorescence response to other biomolecules possibly

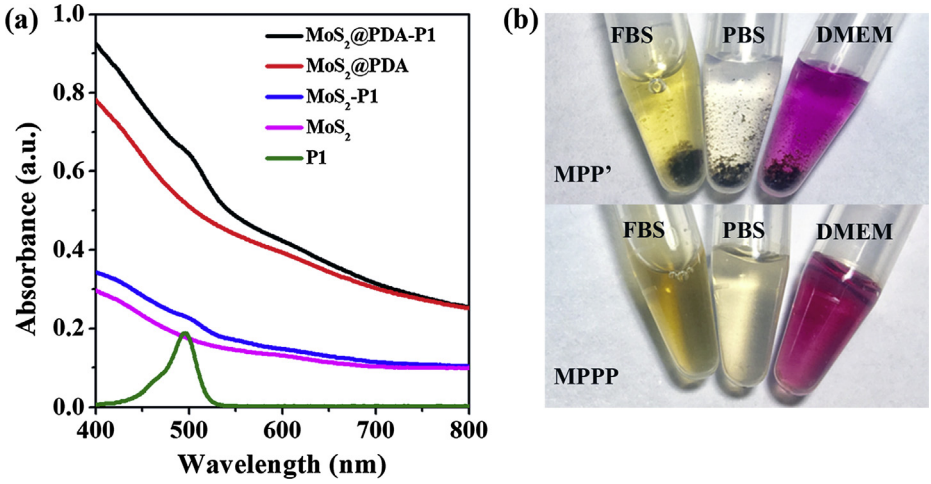

Fig. 3. (a) Ultraviolet–visible-near infrared (UV–vis-NIR) spectra of the caspase-3 substrate peptide (P1), MoS_2@PDA-P1, MoS_2-P1, MoS_2@PDA, and MoS_2 NSs. The concentrations of P1 is 2.4 μM and the concentration of MoS_2 in MoS_2@PDA-P1, MoS_2-P1, and MoS_2@PDA dispersions are all 4.2 μg/mL. (b) Photographs of the MoS_2-PEG-P1/P2 (MPP') and MoS_2@PDA-PEG-P1/P2 (MPPP) NSs dispersed in pure fetal bovine serum (FBS), phosphate buffer saline (PBS, pH = 7.4), and Dulbecco's modified Eagle medium (DMEM) for 36 h at 4 °C. The concentrations of MoS_2 in all of the three samples are 20 μg/mL.

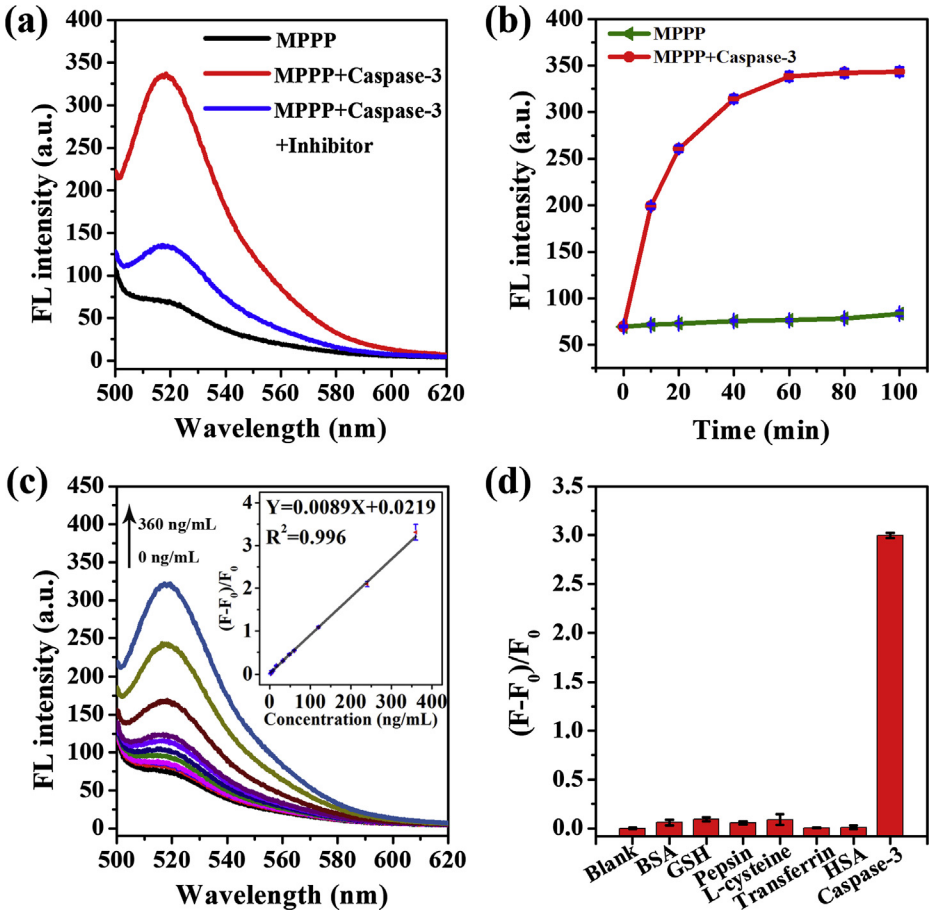

Fig. 4. (a) Fluorescence spectra of the MPPP biosensor (8 μg/mL) in caspase-3 assay buffer, MPPP biosensor (8 μg/mL) with 360 ng/mL of caspase-3, MPPP biosensor (8 μg/mL) with 360 ng/mL of caspase-3 plus 100 μM of caspase-3 inhibitor (Z-DEVD-FMK). (b) Time-dependent fluorescence response of the MPPP biosensor (8 μg/mL) at 518 nm in the absence and presence of caspase-3 (360 ng/mL). (c) Fluorescence response of the MPPP biosensor in the presence of various concentrations of caspase-3. Inset: plot of relative fluorescence intensity changes at 518 nm versus caspase-3 concentrations. (d) Relative fluorescence response of MPPP biosensor at 518 nm to caspase-3, bovine serum albumin (BSA), human serum albumin (HSA), glutathione (GSH), pepsin, L-cysteine, and transferrin. Data are presented as average ± standard deviation (SD) from three independent measurements.

coexisting with caspase-3, including bovine serum albumin (BSA), human serum albumin (HSA), glutathione (GSH), pepsin, L-cysteine, and transferrin (Fig. 4d). Results show that the fluorescence recovery of MPPP biosensor to these species can be neglected, indicating high selectivity of the MPPP biosensor for caspase-3 detection.

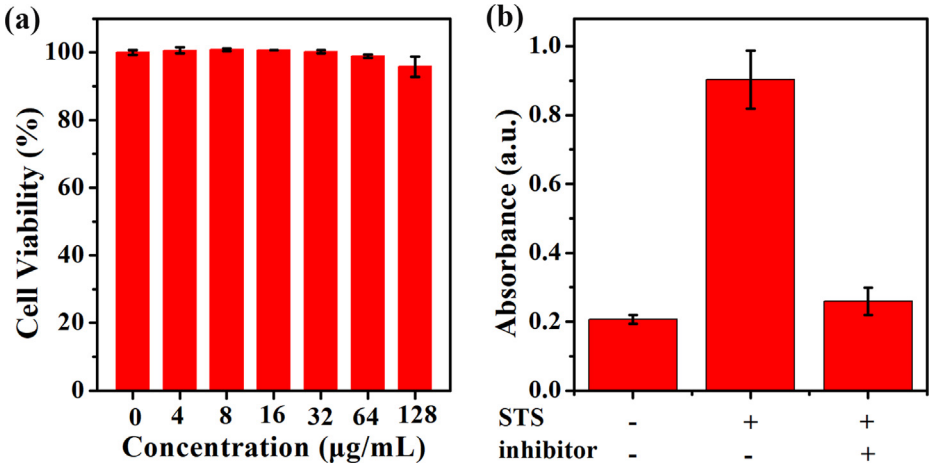

Fig. 5. (a) Viability of HeLa cells after incubation with a range of concentrations of MPPP biosensors for 24 h determined by the LDH-Cytotoxicity Assay Kit. (b) Caspase-3 activity in extracts of HeLa cells treated with STS (2 μM) in the presence and absence of caspase-3 inhibitor Z-DEVD-FMK (100 μM). Data are presented as average ± standard deviation (SD) from three independent measurements.

The cytotoxicity of the MPPP biosensor was examined by the LDH assay using human cervix carcinoma (HeLa) cells as model (Fig. 5a). After incubating with different concentrations of the MPPP biosensor up to 128 μg/mL for 24 h, HeLa cells still maintains viability over 95%, suggesting that the MPPP biosensor possesses good biocompatibility.

Since caspase-3 plays a significant role in cell apoptosis and can be activated by the cell apoptosis inducer of staurosporine (STS), [48] we then investigated whether caspase-3 could be activated in HeLa cells after the treatment of STS by using a commercial Caspase-3 Colorimetric Assay Kit. As shown in Fig. 5b, compared with HeLa cells without STS, the absorbance at 405 nm increases remarkably in apoptotic HeLa cells after treatment with STS (2 μM) for 2 h at 37 °C, suggesting significantly enhanced caspase-3 activity during STS-induced cell apoptosis. In contrast, HeLa cells pretreated with caspase-3 inhibitor (Z-DEVD-FMK, 100 μM) before STS treatment showed no obvious fluorescent signal, indicating that the fluorescence enhancement only happens in the condition of caspase-3 activation.

3.4. Intracellular detection of caspase-3 activity

The intracellular detection of caspase-3 activity by MPPP biosensor was further explored in apoptotic HeLa cells. After incubation with the MPPP biosensor (8 μg/mL) for 3 h at 37 °C, HeLa cells were treated with or without STS for another 4 h. As shown in Fig. 6a (Row 1), there is little fluorescence signal in the absence of STS, indicative of limited caspase-3 activity in nonapoptotic cells [8,9]. In sharp contrast, as shown in Fig. 6a (Row 2), after treated by STS, very bright fluorescent images are achieved, thereby evidencing effective caspase-3 activation and specific peptide cleavage of the MPPP biosensor in apoptotic cells. Furthermore, the control group that HeLa cells pretreated with caspase-3 inhibitor Z-DEVD-FMK before incubating with STS shows little fluorescence signal (Raw 3 in Fig. 6a), confirming the specificity of the MPPP biosensor for intracellular detection of caspase-3 activity. Moreover, the Z-scanning confocal images were taken to visualize the intracellular fluorescence distribution in HeLa cells (Fig. S5). It is apparent that bright green fluorescence exists in the cytoplasm,

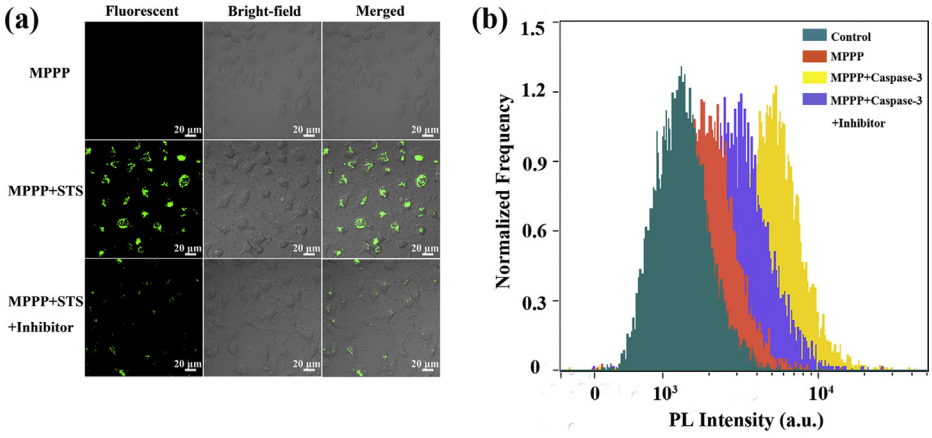

Fig. 6. (a) Confocal laser scanning microscope (CLSM) images of HeLa cells treated with MPPP biosensor (8 μg/mL) for 3 h (Row 1), followed by being treated with STS (2 μM) in the absence (Row 2) and presence (Row 3) of 100 μM of Z-DEVD-FMK. The scale bar is 20 μm. (b) The normalized frequency of HeLa cells with different PL intensity after incubation with no MPPP biosensor (green curve), 8 μg/mL MPPP biosensor (orange curve), 8 μg/mL MPPP biosensor and 2 μM STS in the absence (yellow curve) and presence (purple curve) of 100 μM Z-DEVD-FMK. (For interpretation of the references to colour in this figure legend, the reader is referred to the web version of this article.)

which suggests that the MPPP biosensor can be efficiently translocated to HeLa cells and act as intracellular caspase-3 biosensor for high-contrast imaging of cell apoptosis.

Then the fluorescence signal caused by caspase-3 activation was quantitatively studied by flow cytometry analysis via monitoring the fluorescence of FAM. As shown in Fig. 6b, compared with the control group without any treatment or the group only treated by MPPP biosensor without STS, HeLa cells treated by MPPP biosensor in the presence of STS show the strongest fluorescence signal which is about three times of the group only treated by MPPP biosensor. However, if cells are pretreated by Z-DEVD-FMK before STS treatment, their fluorescence signal decreases by a half. These results are consistent well with the confocal laser scanning microscope (CLSM) imaging results and suggest that the MPPP biosensor with "turn-on" feature has high sensitivity and selectivity for the intracellular detection of caspase-3 activity.

4. Conclusion

In this study, we developed a covalent biofucntionalization strategy of MoS_2 NSs with high conjugation efficiency of peptides by utilizing PDA as nano-bio interface, and constructed an intracellular fluorescent biosensor for caspase-3 activity detection with high sensitivity and selectivity. Benefitting from the covalent biofunctionalization strategy, thiol-containing peptides and PEG can be facilely conjugated to the surface of MoS_2@PDA NSs, which significantly improves the efficiency of peptides conjugation by 3.08 times of that via thiol-metal coordination, and greatly enhances the colloidal stability of MoS_2@PDA NSs in complicated biological environments. In vitro assays revealed that MPPP biosensor possesses high sensitivity and selectivity for the detection of caspase-3 activity with a linear range from 2 ng/mL to 360 ng/mL and a limit of detection (LOD) of 0.33 ng/mL, which is better than previous reports of intracellular fluorescent caspase-3 biosensors [8–10,47]. Confocal laser scanning microscopy and flow cytometry analysis results show that the MPPP biosensor can enter human cervical carcinoma (HeLa) cells and serves as an efficient "turn-on" intracellular fluorescent biosensor for caspase-3 detection. This study not only demonstrates a novel intracellular fluorescent caspase-3 biosensor based on MoS_2 NSs, but also provides a facile and efficient covalent biofucntionalization strategy for the construction of high-performance biosensors, which will further facilitate the construction of 2D multifunctional nanoplatform for various biomedical applications.

Acknowledgements

This work was financially supported by the National Key Research and Development Program of China (2017YFA0205302), the National Natural Science Foundation of China (51503101, 21475064), Program for Changjiang Scholars and Innovative Research Team in University (IRT_15R37), the Key Research and Development Program of Jiangsu (BE2018732), the Natural Science Key Fund for Colleges and Universities in Jiangsu Province (17KJA430011), and Natural Science Foundation of Jiangsu Province (BK20180089).

Appendix A. Supplementary material

Supplementary data to this article can be found online at https://doi.org/10.1016/j.jcis.2019.02.011.

References

[1] A.G. Porter, R.U. Janicke, Emerging roles of caspase-3 in apoptosis, Cell Death Differ. 6 (1999) 99–104.
[2] D.R. McIlwain, T. Berger, T.W. Mak, Caspase functions in cell death and disease, Cold Spring Harbor Perspect. Biol. 5 (2013) a008656.
[3] D. Maysinger, E. Hutter, Nanoparticle-based caspase sensors, Nanomedicine (Lond) 10 (2015) 483–501.
[4] H. Cen, F. Mao, I. Aronchik, R.J. Fuentes, G.L. Firestone, DEVD-NucView488: a novel class of enzyme substrates for real-time detection of caspase-3 activity in live cells, FASEB J. 22 (2008) 2243–2252.
[5] A.P. Guzikowski, J.J. Naleway, C.T. Shipp, R.C. Schutte, Synthesis of a macrocyclic rhodamine 110 enzyme substrate as an intracellular probe for caspase 3 activity, Tetrahedron Lett. 41 (2000) 4733–4735.
[6] D. Altschuh, S. Oncul, A.P. Demchenko, Fluorescence sensing of intermolecular interactions and development of direct molecular biosensors, J. Mol. Recognit. 19 (2006) 459–477.
[7] C.E. Rowland, C.W. Brown, I.L. Medintz, J.B. Delehanty, Intracellular FRET-based probes: a review, Meth. Appl. Fluoresc. 3 (2015) 042006.
[8] H. Wang, Q. Zhang, X. Chu, T. Chen, J. Ge, R. Yu, Graphene oxide-peptide conjugate as an intracellular protease sensor for caspase-3 activation imaging in live cells, Angew. Chem. Int. Ed. 50 (2011) 7065–7069.
[9] X. Zhang, N. Liao, G. Chen, A. Zheng, Y. Zeng, X. Liu, J. Liu, A fluorescent turn on nanoprobe for simultaneous visualization of dual-targets involved in cell apoptosis and drug screening in living cells, Nanoscale 9 (2017) 10861–10868.
[10] K. Boeneman, B.C. Mei, A.M. Dennis, G. Bao, J.R. Deschamps, H. Mattoussi, I.L. Medintz, Sensing caspase 3 activity with quantum dot-fluorescent protein assemblies, J. Am. Chem. Soc. 131 (2009) 3828–3829.
[11] A. Tang, B. Mei, W. Wang, W. Hu, F. Li, J. Zhou, Q. Yang, H. Cui, M. Wu, G. Liang, FITC-quencher based caspase 3-activatable nanoprobes for effectively sensing caspase 3 in vitro and in cells, Nanoscale 5 (2013) 8963–8967.
[12] Y. Li, P. Li, R. Zhu, C. Luo, H. Li, S. Hu, Z. Nie, Y. Huang, S. Yao, Multifunctional gold nanoclusters-based nanosurface energy transfer probe for real-time monitoring of cell apoptosis and self-evaluating of pro-apoptotic Theranostics, Anal. Chem. 88 (2016) 11184–11192.
[13] L. Zhang, J. Lei, J. Liu, F. Ma, H. Ju, In situ activation and monitoring of the evolution of the intracellular caspase family, Chem. Sci. 6 (2015) 3365–3372.
[14] R. Hong, G. Han, J.M. Fernandez, B.J. Kim, N.S. Forbes, V.M. Rotello, Glutathione-mediated delivery and release using monolayer protected nanoparticle carriers, J. Am. Chem. Soc. 128 (2006) 1078–1079.
[15] D.E. Prasuhn, A. Feltz, J.B. Blanco-Canosa, K. Susumu, M.H. Stewart, B.C. Mei, A. V. Yakovlev, C. Loukov, J.M. Mallet, M. Oheim, P.E. Dawson, I.L. Medintz, Quantum dot peptide biosensors for monitoring caspase 3 proteolysis and calcium ions, ACS Nano 4 (2010) 5487–5497.
[16] Q.H. Wang, K. Kalantar-Zadeh, A. Kis, J.N. Coleman, M.S. Strano, Electronics and optoelectronics of two-dimensional transition metal dichalcogenides, Nat. Nanotechnol. 7 (2012) 699–712.
[17] X. Li, J. Shan, W. Zhang, S. Su, L. Yuwen, L. Wang, Recent advances in synthesis and biomedical applications of two-dimensional transition metal dichalcogenide nanosheets, Small 13 (2017) 1602660.
[18] S. Su, J. Chao, D. Pan, L.H. Wang, C.H. Fan, Electrochemical sensors using two-dimensional layered nanomaterials, Electroanalysis 27 (2015) 1062–1072.
[19] X. Zhang, Z. Lai, C. Tan, H. Zhang, Solution-processed two-dimensional MoS2 nanosheets: preparation, hybridization, and applications, Angew. Chem. Int. Ed. 55 (2016) 8816–8838.
[20] C. Zhu, Z. Zeng, H. Li, F. Li, C. Fan, H. Zhang, Single-layer MoS2-based nanoprobes for homogeneous detection of biomolecules, J. Am. Chem. Soc. 135 (2013) 5998–6001.
[21] Y. Zhang, W. Xiu, Y. Sun, D. Zhu, Q. Zhang, L. Yuwen, L. Weng, Z. Teng, L. Wang, RGD-QD-MoS2 nanosheets for targeted fluorescent imaging and photothermal therapy of cancer, Nanoscale 9 (2017) 15835–15845.
[22] T. Liu, C. Wang, X. Gu, H. Gong, L. Cheng, X. Shi, L. Feng, B. Sun, Z. Liu, Drug delivery with PEGylated MoS2 nano-sheets for combined photothermal and chemotherapy of cancer, Adv. Mater. 26 (2014) 3433–3440.
[23] T. Liu, C. Wang, W. Cui, H. Gong, C. Liang, X. Shi, Z. Li, B. Sun, Z. Liu, Combined photothermal and photodynamic therapy delivered by PEGylated MoS2 nanosheets, Nanoscale 6 (2014) 11219–11225.
[24] S.J. Soenen, W.J. Parak, J. Rejman, B. Manshian, (Intra)cellular stability of inorganic nanoparticles: effects on cytotoxicity, particle functionality, and biomedical applications, Chem. Rev. 115 (2015) 2109–2135.
[25] Y. Liu, K. Ai, L. Lu, Polydopamine and its derivative materials: synthesis and promising applications in energy, environmental, and biomedical fields, Chem. Rev. 114 (2014) 5057–5115.
[26] L.Q. Xu, W.J. Yang, K.-G. Neoh, E.-T. Kang, G.D. Fu, Dopamine-induced reduction and functionalization of graphene oxide nanosheets, Macromolecules 43 (2010) 8336–8339.
[27] H. Lee, S.M. Dellatore, W.M. Miller, P.B. Messersmith, Mussel-inspired surface chemistry for multifunctional coatings, Science 318 (2007) 426–430.
[28] L. Yuwen, F. Xu, B. Xue, Z. Luo, Q. Zhang, B. Bao, S. Su, L. Weng, W. Huang, L. Wang, General synthesis of noble metal (Au, Ag, Pd, Pt) nanocrystal modified MoS2 nanosheets and the enhanced catalytic activity of Pd-MoS2 for methanol oxidation, Nanoscale 6 (2014) 5762–5769.
[29] L.H. Yuwen, H. Yu, X. Yang, J. Zhou, Q. Zhang, Y. Zhang, Z. Luo, S. Su, L. Wang, Rapid preparation of single-layer transition metal dichalcogenide nanosheets

via ultrasonication enhanced lithium intercalation, Chem. Commun. 52 (2016) 529–532.
[30] J.M. de la Fuente, C.C. Berry, Tat peptide as an efficient molecule to translocate gold nanoparticles into the cell nucleus, Bioconjugate Chem. 16 (2005) 1176–1180.
[31] M. Zorko, U. Langel, Cell-penetrating peptides: mechanism and kinetics of cargo delivery, Adv. Drug Delivery Rev. 57 (2005) 529–545.
[32] S.S. Chou, B. Kaehr, J. Kim, B.M. Foley, M. De, P.E. Hopkins, J. Huang, C.J. Brinker, V.P. Dravid, Chemically exfoliated MoS_2 as near-infrared photothermal agents, Angew. Chem. Int. Ed. 52 (2013) 4160–4164.
[33] X. Liu, J. Cao, H. Li, J. Li, Q. Jin, K. Ren, J. Ji, Mussel-inspired polydopamine: a biocompatible and ultrastable coating for nanoparticles in vivo, ACS Nano 7 (2013) 9384–9395.
[34] L. Yuwen, Y. Sun, G. Tan, W. Xiu, Y. Zhang, L. Weng, Z. Teng, L. Wang, MoS2@polydopamine-Ag nanosheets with enhanced antibacterial activity for effective treatment of Staphylococcus aureus biofilms and wound infection, Nanoscale 10 (2018) 16711–16720.
[35] Y.K. He, J.T. Wang, H.Q. Zhang, T. Zhang, B. Zhang, S.K. Cao, J.D. Liu, Polydopamine-modified graphene oxide nanocomposite membrane for proton exchange membrane fuel cell under anhydrous conditions, J. Mater. Chem. A 2 (2014) 9548–9558.
[36] L.P. Zhu, J.H. Jiang, B.K. Zhu, Y.Y. Xu, Immobilization of bovine serum albumin onto porous polyethylene membranes using strongly attached polydopamine as a spacer, Colloids Surf. B 86 (2011) 111–118.
[37] M. Jackson, H.H. Mantsch, The use and misuse of FTIR spectroscopy in the determination of protein structure, Crit. Rev. Biochem. Mol. Biol. 30 (1995) 95–120.
[38] Z. Shuxian, W.K. Hall, G. Ertl, H. Knozinger, X-ray photoemission-study of oxygen and nitric-oxide adsorption on MoS2, J. Catal. 100 (1986) 167–175.
[39] M.H. Ryou, Y.M. Lee, J.K. Park, J.W. Choi, Mussel-inspired polydopamine-treated polyethylene separators for high-power li-ion batteries, Adv. Mater. 23 (2011) 3066–3070.
[40] K.H.B.J. Lindberg, G. Johansson, U. Gelius, A. Fahlman, C. Nordling, K. Siegbahn, Molecular Spectroscopy by Means of ESCA II. Sulfur compounds. Correlation of electron binding energy with structure, Phys. Scripta 1 (1970) 286–298.
[41] S.S. Chou, Y.K. Huang, J. Kim, B. Kaehr, B.M. Foley, P. Lu, C. Dykstra, P.E. Hopkins, C.J. Brinker, J. Huang, V.P. Dravid, Controlling the metal to semiconductor transition of MoS2 and WS2 in solution, J. Am. Chem. Soc. 137 (2015) 1742–1745.
[42] W.Z. Zhang, J. Jia, Y.Y. Qiu, K. Pan, Polydopamine-grafted graphene oxide composite membranes with adjustable nanochannels and separation performance, Adv. Mater. Interf. 5 (2018) 1701386.
[43] C. Woghiren, B. Sharma, S. Stein, Protected thiol-polyethylene glycol: a new activated polymer for reversible protein modification, Bioconjug. Chem. 4 (1993) 314–318.
[44] J.P. Badyal, A.M. Cameron, N.R. Cameron, D.M. Coe, R. Cox, B.G. Davis, L.J. Oates, G. Oye, P.G. Steel, A simple method for the quantitative analysis of resin bound thiol groups, Tetrahedron Lett. 42 (2001) 8531–8533.
[45] M. Oishi, A. Tamura, T. Nakamura, Y. Nagasaki, A smart nanoprobe based on fluorescence-quenching PEGylated nanogels containing gold nanoparticles for monitoring the response to cancer therapy, Adv. Funct. Mater. 19 (2009) 827–834.
[46] D. Ren, J. Wang, Z. You, Long-term monitoring of capase-3 activity in living cells based on the FRET probe composed of quantum dot, nanogold and EGF, RSC Adv. 4 (2014) 54907–54918.
[47] Y. Shi, C. Yi, Z. Zhang, H. Zhang, M. Li, M. Yang, Q. Jiang, Peptide-bridged assembly of hybrid nanomaterial and its application for caspase-3 detection, ACS Appl. Mater. Interf. 5 (2013) 6494–6501.
[48] A. Stepczynska, K. Lauber, I.H. Engels, O. Janssen, D. Kabelitz, S. Wesselborg, K. Schulze-Osthoff, Staurosporine and conventional anticancer drugs induce overlapping, yet distinct pathways of apoptosis and caspase activation, Oncogene 20 (2001) 1193–1202.